Front. Energy 2021, 15(3): 772–780
https://doi.org/10.1007/s11708-021-0783-7

RESEARCH ARTICLE

Hongmei WU, Feng LI, Yanqi YUAN, Jing LIU, Liping ZHAO, Peng ZHANG, Lian GAO

Enhancing the photoelectrochemical performance of p-silicon through TiO_2 coating decorated with mesoporous MoS_2

Abstract MoS_2 is a promising electrocatalyst for hydrogen evolution reaction and a good candidate for cocatalyst to enhance the photoelectrochemical (PEC) performance of Si-based photoelectrode in aqueous electrolytes. The main challenge lies in the optimization of the microstructure of MoS_2, to improve its catalytic activity and to construct a mechanically and chemically stable cocatalyst/Si photocathode. In this paper, a highly-ordered mesoporous MoS_2 was synthesized and decorated onto a TiO_2 protected p-silicon substrate. An additional TiO_2 necking was introduced to strengthen the bonding between the MoS_2 particles and the TiO_2 layer. This meso-MoS_2/TiO_2/p-Si hybrid photocathode exhibited significantly enhanced PEC performance, where an onset potential of + 0.06 V (versus RHE) and a current density of − 1.8 mA/cm^2 at 0 V (versus RHE) with a Faradaic efficiency close to 100% was achieved in 0.5 mol/L H_2SO_4. Additionally, this meso-MoS_2/TiO_2/p-Si photocathode showed an excellent PEC ability and durability in alkaline media. This paper provides a promising strategy to enhance and protect the photocathode through high-performance surface cocatalysts.

Keywords photoelectrocatalysis, hydrogen evolution, Si photocathode, mesoporous MoS_2

Received Mar. 30, 2021; accepted Jul. 30, 2021; online Sept. 15, 2021

Hongmei WU, Feng LI, Yanqi YUAN, Jing LIU (✉), Liping ZHAO, Peng ZHANG (✉), Lian GAO
School of Materials Science and Engineering, Shanghai Jiao Tong University, Shanghai 200240, China
E-mail: liujing2014@sjtu.edu.cn (Jing LIU);
pengzhang2010@sjtu.edu.cn (Peng ZHANG)

Special issue—Photocatalysis: From Solar Light to Hydrogen Energy (Guest Editors: Wenfeng SHANGGUAN, Akihiko KUDO, Zhi JIANG, Yuichi YAMAGUCHI)

1 Introduction

Along with the high-speed economic development and rapid population growth, energy and environmental issues are becoming the focus of global attention. As a clean, carbon-free fuel, H_2 is considered as an ideal energy carrier to replace fossil fuels. Solar-driven water splitting has been proven to be a promising route toward renewable hydrogen production [1–3], which attracts ever-increasing attention for the development of high-performance and cost-effective photoelectrochemical (PEC) devices for hydrogen evolution reaction (HER). In this regard, silicon (Si) is demonstrated as an ideal candidate for PEC HER applications with its narrow bandgap (E_g = 1.1 eV), high earth abundance, low cost, and large-scale production [4,5]. Although significant progress has been made since Si was used as a photovoltaic material, the PEC efficiency and chemical stability are largely limited by its surface corrosion, especially in aqueous electrolytes, as well as extremely sluggish HER kinetics [1,6,7].

An efficient strategy to suppress the corrosion of Si photoelectrode during PEC reaction is to deposit a protective layer on the surface of Si. A variety of materials, such as Al_2O_3, TiO_2, NiO_x, and SiO_x, have been used [6–10], among which, TiO_2 is a common material to protect Si electrodes due to its superior electronic conductivity, high corrosion resistance, and chemical stability in a broad range of pH [11–13].

Sluggish HER kinetics of Si, resulting from its high hydrogen adsorption Gibbs free energy (ΔGH), is another big issue of Si photoelectrodes [14]. Therefore, substantial research endeavors have been dedicated to designing PEC Si photocathodes with enhanced HER activity. It is reported that a passivation layer, e.g., a TiO_2 layer, can help fix surface defects of Si-based photocathode to reduce surface carrier recombination and hence improve the HER [11,15]. In addition, decorating the surface of photocathode with a cocatalyst can accelerate the reaction

between the photo-generated carriers and the electrolyte [16,17]. Numerous methods of designing Si-based photocatalysts for high-efficiency photocatalytic systems mainly focusing on loading precious metals on p-Si surfaces have been proposed [5,12,18–20]. However, the high cost and scarcity of noble metals pose tremendous obstacles to their further application, though these precious metals show excellent catalytic activity at a low overpotential. As a consequence, extensive efforts have been made to develop earth-abundant non-noble metal HER catalysts [13,21,22].

Graphene-like MoS_2, a layered transitional metal sulfide with a direct band gap, has been extensively investigated as a cocatalyst for Si photocathodes owing to its unique optical, electrical, and chemical properties [14,16,23–25]. However, the active sites of 2H-MoS_2 are mainly concentrated at its edges, while the basal plane (0001) of MoS_2 is inert to HER [25,26]. Therefore, designing the morphology of MoS_2 and tuning its size with more exposed active edges are effective strategies to boost its HER performance [25,27–29]. For example, Kibsgaard and coworkers successfully constructed a MoS_2 with a 3D network structure and a highly ordered double-gyroid (DG) morphology by using porous silicon as the template. The DG meso-structured MoS_2 possesses a fully contiguous large-area thin film with a greater fraction of catalytically active sites that are favorable to charge transport and diffusion [29]. Wang et al. demonstrated that the edge-terminated structure of ultrathin MoS_2 nanoflakes exhibited an enhanced H_2 production rate, because the ultra-small MoS_2 flakes substantially increased the ratio of exposed active edges [28]. To sum up, engineering an active site-rich structure by tuning the molecular size and creating a mesoporous network structure by morphological modulation at nanoscale are of great significance for MoS_2 to improve the surface properties and charge carrier transfer. Nevertheless, it is still challenging to prepare ordered mesoporous MoS_2 with a maximum of active edge sites.

Furthermore, the method to construct cocatalyst/Si photoelectrode has a significant influence on its PEC performance. The cocatalyst should be bonded onto the surface with enough strength to prevent separation and failure during PEC reaction. Meanwhile, the photogenerated carriers are able to be well transferred from Si to the cocatalyst.

Herein, a commercial planar Si based hybrid photocathode with a TiO_2 passivation layer and ordered mesoporous MoS_2 cocatalyst is reported. The highly-ordered mesoporous MoS_2 was successfully synthesized by using a facile and controllable template method, which had a superior electrocatalytic performance in HER. The TiO_2 worked both as an effective protective layer against corrosion of Si electrode, passivation layer and as an efficient carrier transfer path. This meso-MoS_2/TiO_2/p-Si architecture was constructed using a post-necking strategy to ensure the structural stability of the hybrid photocathode. As a result, an excellent PEC performance was achieved, with an onset potential of + 0.06 V (versus RHE, V_{RHE}), a current density of − 1.8 mA/cm^2 at 0 V_{RHE}, and a Faradaic efficiency close to 100% in acidic media. Very recently, Li et al. [30] have chosen MoS_2 as a cocatalyst to construct a Si/TiO_2/MoS_2 photoelectrode and obtained a photocurrent density of − 0.24 mA/cm^2 at 0 V_{RHE}, an onset potential of 0.42 V_{RHE}, and a stability of more than 8 h in 0.5 mol/L H_2SO_4 solution. Compared with the work mentioned above, such superior HER efficiency and chemical stability suggested that the present paper provides a promising strategy for fabricating Si-based photocathodes by loading mesoporous cocatalysts.

2 Experimental section

2.1 Materials

The thiourea (CH_4N_2S, ⩾ 99.0%), sodium molybdate dihydrate ($Na_2MoO_4 \cdot 2H_2O$, ⩾ 99.0% purity), citric acid monohydrate ($C_6H_8O_7 \cdot H_2O$, 99.5%), potassium hydroxide (KOH, 95%), hydrofluoric acid (HF, ⩾ 40.0%), acetone (C_3H_6O, ⩾ 99.5%), sulfuric acid (H_2SO_4, ⩾ 98%), titanium tetrachloride ($TiCl_4$, ⩾ 98.0%) were purchased from Sinopharm Chemical Reagent Co., Ltd. The ethanol (C_2H_5OH, ⩾ 99.7%) and the hexane ($CH_3(CH_2)_4CH_3$, ⩾ 97.0%) were obtained from Shanghai Titan Scientific Co., Ltd. The methanol (CH_4O, ⩾ 99.9%) and the potassium hexachloroplatinate (K_2PtCl_6, ⩾ 98%) were purchased from Shanghai Aladdin Biochemical Technology Co., Ltd. All reagents used in this study were employed without any further treatment. Ultra-pure Milli-Q water was used in the entire experimental process.

2.2 Fabrication of mesoporous and nanostructured MoS_2 powders

The mesoporous MoS_2 was synthesized using a nanocasting method with KIT-6 as the template. Typically, 500 mg KIT-6 powder was added into 40 mL $CH_3(CH_2)_4CH$ and stirred at 50°C for 2 h. The cubic *Ia*3*d* mesoporous silica, KIT-6, was prepared according to Refs. [13,31]. Then, the precursor solution of MoS_2 (0.5 mL) was dispersed into the above solution and stirred for 4 h. The precursor solution of MoS_2 was obtained by dissolving CH_4N_2S (160 mg) and $Na_2MoO_4 \cdot 2H_2O$ (200 mg) in 1 mL Milli-Q water. After being dried under vacuum at 60°C for 10 h, the mixture was calcined at 600°C at a slow ramping rate of 2°C/min for 5 h under Ar flow. Subsequently, the as-obtained MoS_2/KIT-6 was dispersed in 5% HF aqueous solution to remove KIT-6 template. Finally, the mesoporous MoS_2 was obtained after washing by using Milli-Q water and ethanol several times, and then dried at 60°C

overnight. The synthesis procedures are illustrated in Fig. 1. The meso-Pt was prepared by the same process by using K_2PtCl_6 as precursor.

For comparison, the nonporous nanostructured MoS_2 was fabricated by using a hydrothermal process. The synthesis was conducted as follows: 25 mg of $Na_2MoO_4 \cdot 2H_2O$ and 35 mg CH_4N_2S were dispersed in 35 mL Milli-Q water via 10-min ultrasonic treatment before 235 mg $C_6H_8O_7 \cdot H_2O$ was added. After another 10 min of ultrasonic dispersion, the mixture was then transferred into a 50 mL Teflonlined stainless steel autoclave, sealed, and heated at 200°C for 21 h. After being naturally cooled down to room temperature, the precipitate was washed with Milli-Q water and ethanol thoroughly, then dried at 60°C overnight.

2.3 Fabrication of TiO_2/p-Si

Czochralski (CZ) p-type (100) silicon wafers (150 mm× 150 mm× 0.65 mm, ρ = 5–15 Ω·cm) were used for this work. First, the Si chips with a size of 1 cm × 2 cm were ultrasonically cleaned in Milli-Q water, ethanol, and acetone for 30 min, respectively. The surface native oxide layer was then removed with 5% HF aqueous solution for 10 min, followed by atomic layer deposition process (ALD, Ultratech, Savannah 100, USA). TiO_2 passivation layer with a thickness of 5 nm was deposited onto p-Si substrates at 150°C and a stream of N_2 (20 sccm) using tetrakis-dimethylamino titanium (TDMAT, 0.1 s pulse) and H_2O (0.015 s pulse) as the Ti and O precursors, respectively.

2.4 Fabrication of photoelectrodes

The meso-MoS_2/TiO_2/p-Si was obtained by using the spin-coating method. After the surface of TiO_2/p-Si was cleaned by a drop of methanol solution, three drops of meso-MoS_2 diluted solution (2 mg meso-MoS_2 powder being added in 100 μL C_2H_5OH and 100 μL CH_3OH) were evenly spin-coated onto the surface of TiO_2/p-Si at 3000 r/min for 60 s, followed by a drop of 0.01 mol/L $TiCl_4$ methanol solution. After that, the meso-MoS_2/TiO_2/p-Si was dried at 60°C for 10 min, and then sintered at 350°C at a heating rate of 20°C/min for 10 min under Ar flow. An Ohmic contact was established by coating an InGa alloy in the backside of p-Si and then adhering a Cu wire with Ag paste. Afterwards, the entire backside and the edges of p-Si were sealed by epoxy, while an area of 1 cm^2 on the front of p-Si was exposed for PEC tests. The nano-MoS_2/TiO_2/p-Si and meso-Pt/TiO_2/p-Si were prepared by the same process.

2.5 Characterization

The morphologies and composition of prepared samples were characterized by field-emission scanning electron microscopy (FE-SEM, Tescan MIRA3), transmission electron microscopy (TEM, FEI Tecnai G2) and High-resolution TEM (HRTEM, TALOS F200X). The energy dispersive X-ray spectroscopy (EDS) mapping profiles were also conducted in the FE-SEM (Tescan MIRA3). The structural properties were detected using X-ray diffraction diffractometer (XRD, Rigaku D/max 2550) with Cu Kα radiation (λ = 1.5418 Å) operated at an acceleration voltage of 40 kV.

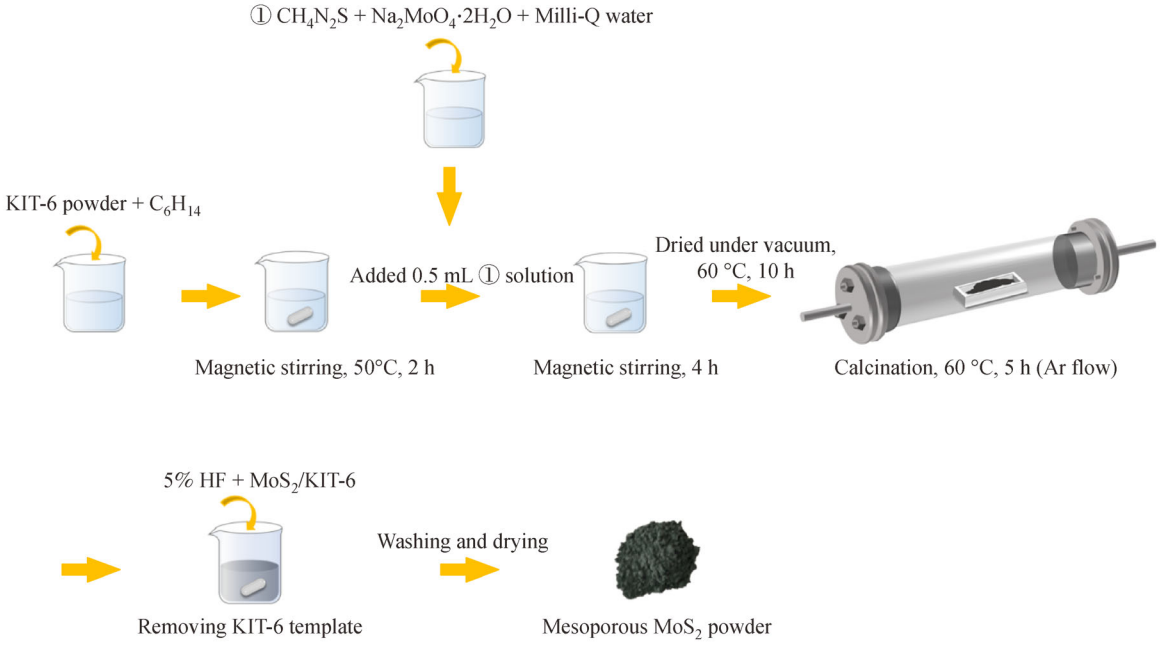

Fig. 1 Procedures for the synthesis of mesoporous MoS_2.

2.6 Electrochemical and photoelectrochemical measurements

For electrochemical measurements, a glassy carbon electrode (0.07 cm^2) covered with catalyst was used as the working electrode. Typically, 2 mg of resultant product was dispersed in the mixture of 8 μL Nafion solution (5% (mass percentage), Dupont Corporation) and 200 μL water-ethanol solution (volume ration:1:1) via 60-min ultrasonic oscillation to acquire a homogeneous ink. Then, 6 μL of the ink was pipetted on a GC electrode and dried naturally overnight.

A three-electrode mode served as electrochemical and PEC measurements, with a multifunctional electrochemical analysis instrument (Bio-logic VMP3), using 0.5 mol/L H_2SO_4 and 1 mol/L KOH aqueous solution as the electrolyte. In the acid solution, a Pt wire and an Ag/AgCl electrode were used as the counter and reference electrodes, respectively. A graphite rod (d = 5 mm) and a Hg/HgO electrode served as the counter and reference electrodes in the alkaline electrolyte, respectively. Photoelectrochemical measurements were evaluated under a 300 W Xe lamp with an optical filter ($\lambda > 400$ nm) as the visible light source (AM 1.5 G one sun illumination) at room temperature. The electrochemical impedance spectroscopy (EIS) was performed from 200 kHz to 0.1 Hz at a bias of –0.1 V_{RHE} and a sinusoidal voltage of 5 mV.

3 Results and discussion

The morphologies of the meso-MoS_2/TiO_2/p-Si and pristine nano-MoS_2 samples were characterized by FE-SEM, TEM and HRTEM. As demonstrated in Figs. 2(a), S1(a), and S1(d), the mesoporous MoS_2 particles, MoS_2 nanoparticles, and mesoporous Pt particles were uniformly distributed on the entire surface of the p-Si substrate. Moreover, obvious MoS_2 nanoflowers can be observed, but they all aggregated together and formed MoS_2 clusters (Fig. S1(c)). The low magnification TEM image (Fig. 2(b))

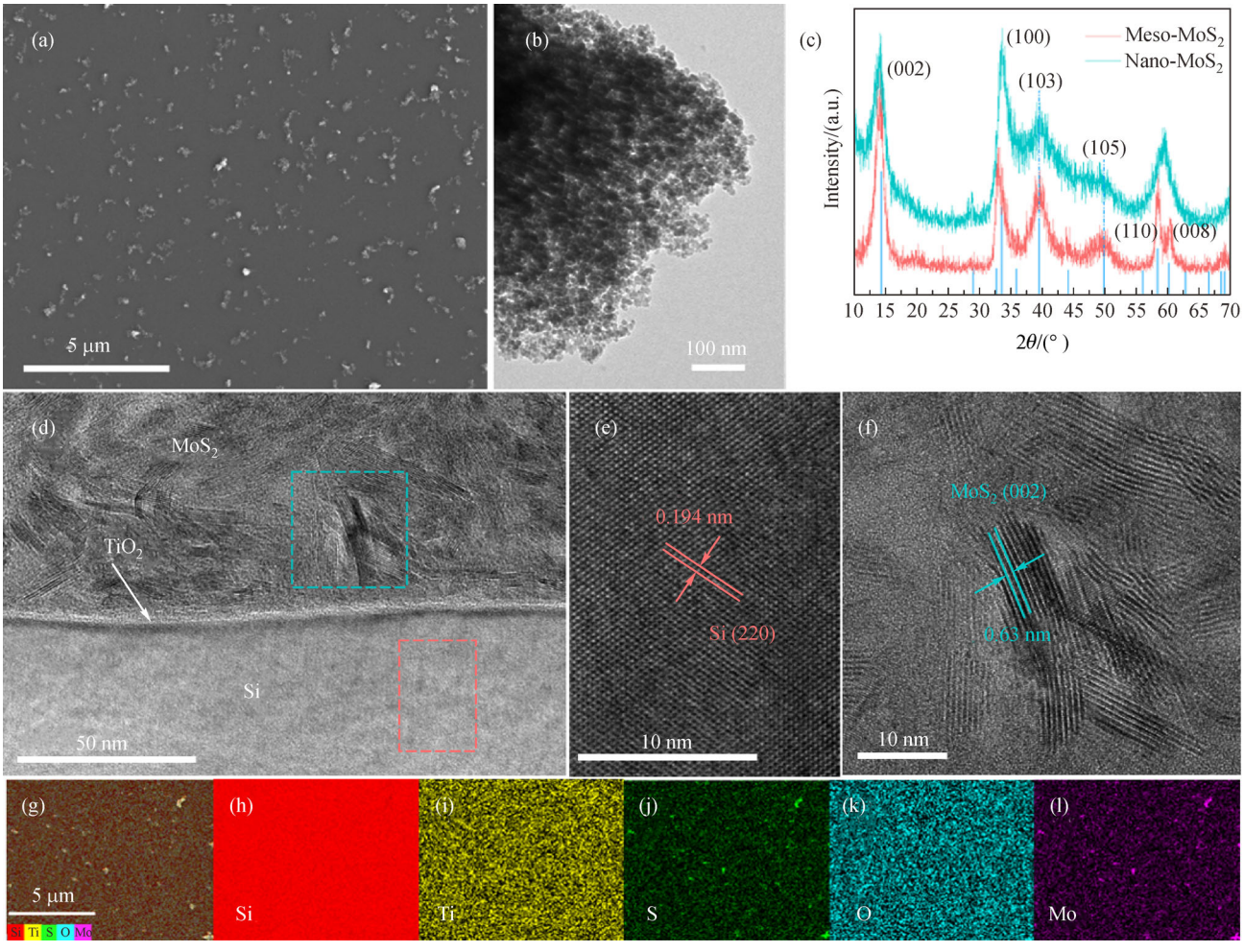

Fig. 2 Characterization of the as-prepared samples.
(a) SEM images of meso-MoS_2/TiO_2/p-Si; (b) TEM image of meso-MoS_2; (c) XRD patterns of meso-MoS_2 and nano-MoS_2; (d) cross-sectional HRTEM images of meso-MoS_2/TiO_2/p-Si, (e) p-Si; (f) meso-MoS_2; (g–l) the corresponding elemental mappings of meso-MoS_2/TiO_2/p-Si.

exhibits an ordered mesoporous structure composed of ultra-thin and ultra-small MoS_2 sheets, which provides a large surface area and more active sites for HER. As displayed in Fig. 2(d) and Fig. S1(b), the cross-sectional high-resolution TEM (HRTEM) images clearly reveals the tandem structure of the hybrid photoelectrodes, which contains the MoS_2 particles (meso-MoS_2 or nano-MoS_2 particles) anchored on an amorphous-structured TiO_2 thin film and the TiO_2 thin layer coated on the surface of the p-Si. The well-resolved lattice fringes with interplanar spaces of 0.194 nm and 0.63 nm can be indexed to the (220) plane of Si and the (002) plane of MoS_2, respectively (Figs. 2(e) and 2(f)). The EDS analysis of the synthesized meso-MoS_2/TiO_2/p-Si (Figs. 2(g)–2(l)) confirms the homogeneous dispersion of Mo and S atoms, as well as Ti and O atoms, demonstrating the formation of meso-MoS_2/TiO_2/p-Si. The XRD patterns of meso-MoS_2 and nano-MoS_2 are depicted in Fig. 2(c). The peak positions at 2θ = 14.3°, 32.6°, 39.5°, 49.7°, 58.3°, and 60.1° can be indexed to (002), (100), (103), (105), (110), and (008) planes of the hexagonal MoS_2 phase (JCPDS 37-1492), further demonstrating the successful preparation of MoS_2. For meso-MoS_2, the diffraction peak of (002) shifted slightly to the left, indicating an expanded interlayer, which is beneficial for enhancing the charge transfer rate. In addition, theoretical studies have indicated that increasing the interlayer spacing of MoS_2 can reduce the Gibbs free energy of hydrogen adsorption (DGH) compared with the non-expanded pristine MoS_2, which benefits the desorption of hydrogen from the surfaces of cocatalysts [32,33]. As for nano-MoS_2, the diffraction peaks were relatively weaker than that of meso-MoS_2 and the peaks at 2θ = 58.3° and 60.1° merged into one broad peak, revealing a low crystalline degree.

To provide more information about the enlarged surface area of meso-MoS_2, the specific surface area and porous structure were characterized by nitrogen adsorption-desorption isotherms (Fig. 3). The isotherm curve belongs to type IV with a hysteresis loop and sharp changed adsorption/desorption lines, indicative of large cylindrical-like mesopores in a narrow range of size. The BET surface area of meso-MoS_2 is 587.613 m^2/g, which is much higher than that of nano-MoS_2 (10.530 m^2 /g). Moreover, the pore size distribution (PSD, inset of Fig. S2(a)) of meso-MoS_2 measured by the Barrett-Joiner-Halenda method is in a relatively narrow distribution, which is mainly centered at 3.82 nm. Comparatively, the PSD of nano-MoS_2 was dispersed and has an average pore size of 2.46 nm, less than that of meso-MoS_2, as exemplified in Fig. S2(b) and the inset. The significant increase in the specific surface area and the formation of mesoporous structure verify the expected design again, which might be conducive to charge transfer and hydrogen diffusion, as well as increasing the exposure of active edges.

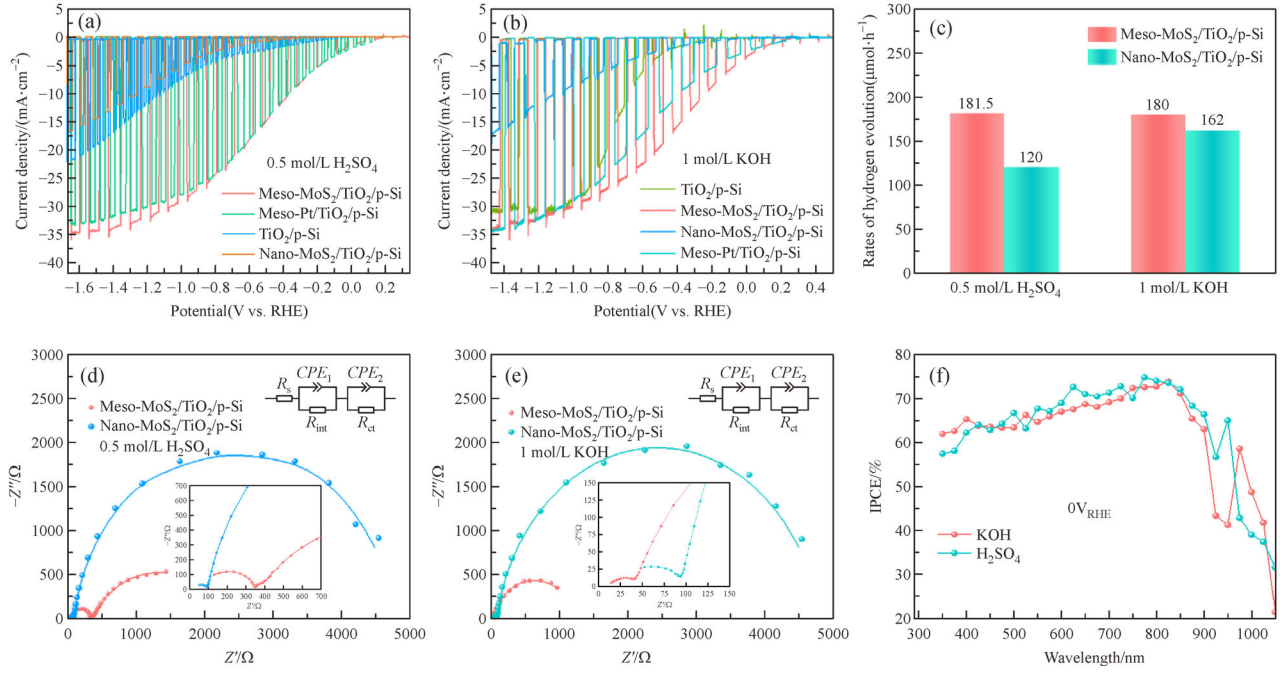

Fig. 3 PEC performance of the as-prepared photoelectrodes.

(a) Chopped LSVs of TiO_2/p-Si, meso-MoS_2/TiO_2/p-Si, meso-Pt/TiO_2/p-Si and nano-MoS_2/TiO_2/p-Si in 0.5 mol/L H_2SO_4; (b) chopped LSVs of TiO_2/p-Si, meso-MoS_2/TiO_2/p-Si, meso-Pt/TiO_2/p-Si and nano-MoS_2/TiO_2/p-Si in 1.0 mol/L KOH; (c) photoelectrocatalytic H_2 generation rates of meso-MoS_2/TiO_2/p-Si and nano-MoS_2/TiO_2/p-Si photoelectrodes in 0.5 mol/L H_2SO_4 and 1.0 mol/L KOH solutions; (d) Nyquist plots recorded at − 0.1 V_{RHE} in 0.5 mol/L H_2SO_4; (e) Nyquist plots recorded at − 0.1 V_{RHE} in 1.0 mol/L KOH; (f) IPCE of meso-MoS_2/TiO_2/p-Si photoelectrodes at 0 V_{RHE} in 0.5 mol/L H_2SO_4 and 1.0 mol/L KOH solutions.

The PEC performance of the prepared photocathodes was first evaluated in 0.5 mol/L H_2SO_4 electrolyte under simulated AM 1.5 G one sun illumination ($\lambda > 400$ nm), as manifested in Fig. 3(a). Compared with all the samples, meso-MoS_2/TiO_2/p-Si yields the highest photocurrent density of –1.8 mA/cm^2 at 0 V_{RHE} except meso-Pt/TiO_2/p-Si (–2.1 mA/cm^2) and the lowest onset potential of 0.06 V_{RHE} (j = –1 mA/cm^2). Besides, the saturation current density (34.4 mA/cm^2 at 1.4 V_{RHE}) of meso-MoS_2/TiO_2/p-Si even surpasses the value of meso-Pt/TiO_2/p-Si at the same potential. These results suggest that the introduction of meso-MoS_2 promotes the charge migration process, endowing the photoelectrode with an improved photocatalytic activity [34]. Note that the HER performance of nano-MoS_2/TiO_2/p-Si is worse than that of TiO_2/p-Si, presumably because the nano-MoS_2 dispersed on the surface of p-Si affects the light absorption and hinders the hydrogen evolution process of the composite photoelectrode. After loading the cocatalyst, no matter what kind of composite photoelectrode it is, there is a light blocking effect, including meso-Pt/TiO_2/p-Si and meso-MoS_2/TiO_2/p-Si. The HER photoelectrocatalytic performance of the photoelectrodes are not only influenced by the light absorption of the silicon substrate, but also by the properties and structure of the cocatalyst themselves. However, meso-Pt/TiO_2/p-Si and meso-MoS_2/TiO_2/p-Si still show excellent PEC performance under the effect of light blocking, indicating the advantages of mesoporous structure.

The HER photoelectrocatalytic activity was also investigated in the presence of a 1.0 mol/L KOH aqueous solution, as displayed in Fig. 3(b). Similar to the acidic solution, nano-MoS_2/TiO_2/p-Si shows a poor HER activity in alkaline media with an onset overpotential at 0.29 V_{RHE}. In contrast, meso-MoS_2/TiO_2/p-Si requires only 0.14 V_{RHE}, which is much smaller than that of TiO_2/p-Si and nano-MoS_2/TiO_2/p-Si. Furthermore, the meso-MoS_2/TiO_2/p-Si composite photocathode shows a current density of –3.3 mA/cm^2 at 0 V_{RHE}, which is even higher than that of meso-Pt/TiO_2/p-Si (–2.5 mA/cm^2 at 0 V_{RHE}).

Moreover, the H_2 production from the meso-MoS_2/TiO_2/p-Si photocathode was collected to evaluate the Faradaic efficiencies at a bias of 0.1 V_{RHE}. As displayed in Fig. 3(c), the H_2 generation rate was 181.5 μmol/h in acidic electrolyte and 180 μmol/h in alkaline media, respectively; the corresponding Faradaic efficiencies were both close to 100% (97.4% in 0.5 mol/L H_2SO_4, 96.5% in 1.0 mol/L KOH), revealing that the generated photocurrent is indeed derived from HER. Compared with meso-MoS_2/TiO_2/p-Si, nano-MoS_2/TiO_2/p-Si photoelectrodes exhibit lower H_2 production rates both in acidic (120 μmol/h) and alkaline solution (162 μmol/h) at an applied potential of –0.5 V_{RHE} and the corresponding Faradaic efficiencies were 64.3% and 86.8%, respectively. Figure 3(f) shows the changes of IPCE values in different electrolytes from 350 nm to 975 nm. In acidic solution, the IPCE values of meso-MoS_2/TiO_2/p-Si photoelectrodes mostly surpass 57% in the range of 350–875 nm, and peak at 75% or so at 775 nm. In the alkaline solution, the majority of the IPCE value is above 60%, and reaches the maximum value of 73.5% at 825 nm.

The faster reaction kinetics is manifested by EIS under simulated AM 1.5 G one sun illumination (Figs. 3(d) and 3(e)). The Nyquist plots are fitted with the equivalent model, as shown in the insets of Figs. 3(d) and 3(e). Therein, R_s represents a series resistance of the whole synthetic circuit. R_{ct_1}-CPE_1 simulates the resistances of the charge transfer process at the photoelectrode/electrolyte interface and the double layer of the nonideal capacitance. R_{ct_2}-CPE_2 is closely related to the charge transfer resistances at the TiO_2/Si and cocatalyst/TiO_2 interfaces. Commonly, a smaller arc radius indicates a lower interface resistance. It should be noted that the arc radii of meso-MoS_2/TiO_2/p-Si photoelectrodes at low-frequency ranges are significantly smaller than those of nano-MoS_2/TiO_2/p-Si photocathodes in both electrolytes, suggesting that this unique mesoporous architecture reduces diffusion limitations of reactants and products (such as H^+ and H_2) and also effectively enhances the separation and transfer efficiency of photoelectrons during HER.

The PEC stability test of meso-MoS_2/TiO_2/p-Si was performed by a chronoamperometry test at a fixed applied potential of –0.1 V_{RHE} in 1 mol/L KOH and –0.15 V_{RHE} in 0.5 mol/L H_2SO_4, respectively. As illustrated in Fig. 4(a), the current density was maintained at (–6±0.2) mA/cm^2 for more than 18 h in 1 mol/L KOH, and (–4±0.2) mA/cm^2 for a duration of 30 h in 0.5 mol/L H_2SO_4, indicating that the as-prepared meso-MoS_2/TiO_2/p-Si photoelectrode possesses an excellent stability either in acidic media or alkaline media, which can be attributed to the TiO_2 protective layer and the post-necking strategy. After 30 h of test in 0.5 mol/L H_2SO_4, as shown in Fig. 4(b), meso-MoS_2 particles were still dispersed on the surface of p-Si, indicating that the catalyst can be stably anchored on the silicon surface under the protection of TiO_2 layer. In addition, coarser particles were observed below the meso-MoS_2 particles, which may be caused by the corrosion of the p-Si surface during the long-term testing. For comparison, the durability results of nano-MoS_2/TiO_2/p-Si photoelectrode in both two electrolytes were also collected, as shown in Fig. S4, the current density continued to increase within 40 h. After the test, it was observed that the surface of the photoelectrode was severely corroded. Therefore, the increased current density during the test was caused by the corrosion in the surface of the photocathode, indicating that the nano-MoS_2/TiO_2/p-Si photocathodes have a poor stability.

Because the proton reduction reaction on the cocatalyst surface is an important step for photoelectrocatalytic HER, the performance of surface reduction reaction has a great influence on the efficiency of HER. To understand the impact of cocatalyst morphology on the PEC performance of the composite photoelectrodes, the HER electrocatalytic

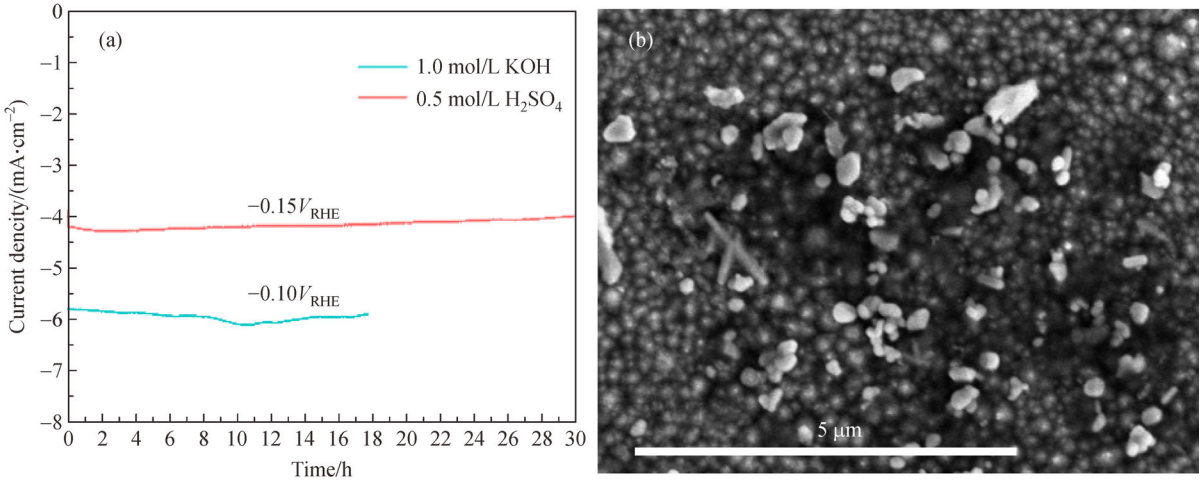

Fig. 4 Stability tests and the corresponding morphology changes of meso-MoS_2/TiO_2/p-Si photocathode.
(a) Durability measurements of meso-MoS_2/TiO_2/p-Si photocathodes in 0.5 mol/L H_2SO_4 and 1.0 mol/L KOH solutions; (b) SEM image of meso-MoS_2/TiO_2/p-Si after 30 h test in 0.5 mol/L H_2SO_4 solution.

activities of meso-MoS_2 were evaluated in 0.5 mol/L H_2SO_4 and 1.0 mol/L KOH, respectively. For comparison, commercial Pt-C (20%), nano-MoS_2, and bare GC were also investigated under the same conditions. As displayed in Figs. 5(a) and 5(b), Pt-C exhibits the lowest onset overpotentials (j = –1 mA/cm^2) in both two electrolytes (–0.028 V_{RHE} in 0.5 mol/L H_2SO_4 and –0.031 V_{RHE} 1.0 mol/L KOH). Except for Pt-C, the meso-MoS_2 electrocatalyst shows the lowest onset overpotentials with –0.22 V_{RHE} in acidic electrolyte and –0.20 V_{RHE} in alkaline solution, which are smaller than the corresponding values of nano-MoS_2 (–0.24 V_{RHE} in 0.5 mol/L H_2SO_4 and –0.24 V_{RHE} in 1.0 mol/L KOH). A lower overpotential at the same current density for meso-MoS_2 indicates a lower potential energy loss, resulting in a higher PEC rate for the meso-MoS_2/TiO_2/p-Si photocathode during proton reduction reaction. The results suggest that the enlarged surface area and ultra-small meso-MoS_2 sheets maximizes the exposure active edge sites, which promotes the surface reduction reaction of the as-prepared photocathode. In addition, the unique mesoporous structure and larger pore size of meso-MoS_2 than that of nano-MoS_2 are more favorable for the diffusion of ions and hydrogen, thus increasing H_2 production efficiency.

To identify the real active surface area of the cocatalyst, ECSA measurements were evaluated from the electrochemical double-layer capacitance (C_{dl}) by collecting the cyclic voltammetry (CV) results in a non-HER potential region (0.02–0.12 V_{RHE} in KOH and 0.01–0.11 V_{RHE} in 0.5 mol/L H_2SO_4) at different scan rates (Figs. 5(a), 5(b), and S3). The C_{dl} values could be obtained by plotting the ΔJ ($J_{anodic} - J_{cathodic}$) at 0.1 V_{RHE} against the scan rates, in which the slope is twice that of C_{dl}. The C_{dl} values of meso-MoS_2 are 22.9 mF/cm^2 in acidic media (Fig. 5(a)) and 9.2 mF/cm^2 in alkaline solution (Fig. 5(b)) respectively, substantially larger than those of nano-MoS_2 (17.5 mF/cm^2 in 0.5 mol/L H_2SO_4, and 5.5 mF/cm^2 in 1.0 mol/L KOH), and the corresponding ECSAs are 572.5 cm^2, and 230.0 cm^2, respectively, indicating that the unique mesoporous-structured MoS_2 could provide a much larger effective surface area and active edge sites for surface reduction reaction of the composite photocathodes, as well as a rapid transport channel for ions and gas diffusion, thus contributing to an enhanced catalytic activity.

The above results demonstrate that the meso-MoS_2 cocatalyst can greatly promote the PEC activity of the hybrid photocathodes and can be a promising alternative to noble metal based cocatalysts.

4 Conclusions

In summary, this paper has demonstrated a Si photocathode for enhanced PEC water splitting by using a highly-ordered mesoporous MoS_2 structure as a novel cocatalyst of p-Si. The mesoporous structure synthesized by a facile and controllable method exposed abundant active sites, which greatly accelerated the HER kinetics. In addition, the formation of this mesoporous structure promoted the charge transfer and hydrogen evolution process. Moreover, a TiO_2 protective layer was deposited on the p-Si substrate, and an additional TiO_2 necking was introduced to strengthen the bonding between the MoS_2 particles and the TiO_2 layer. As a consequence, the prepared meso-MoS_2/TiO_2/p-Si hybrid photocathode exhibits an excellent PEC performance and durability in both acidic and alkaline solutions. These strategies provide helpful guidelines for engineering highly efficient catalysts and PEC photoelectrodes with a superior corrosion resistance.

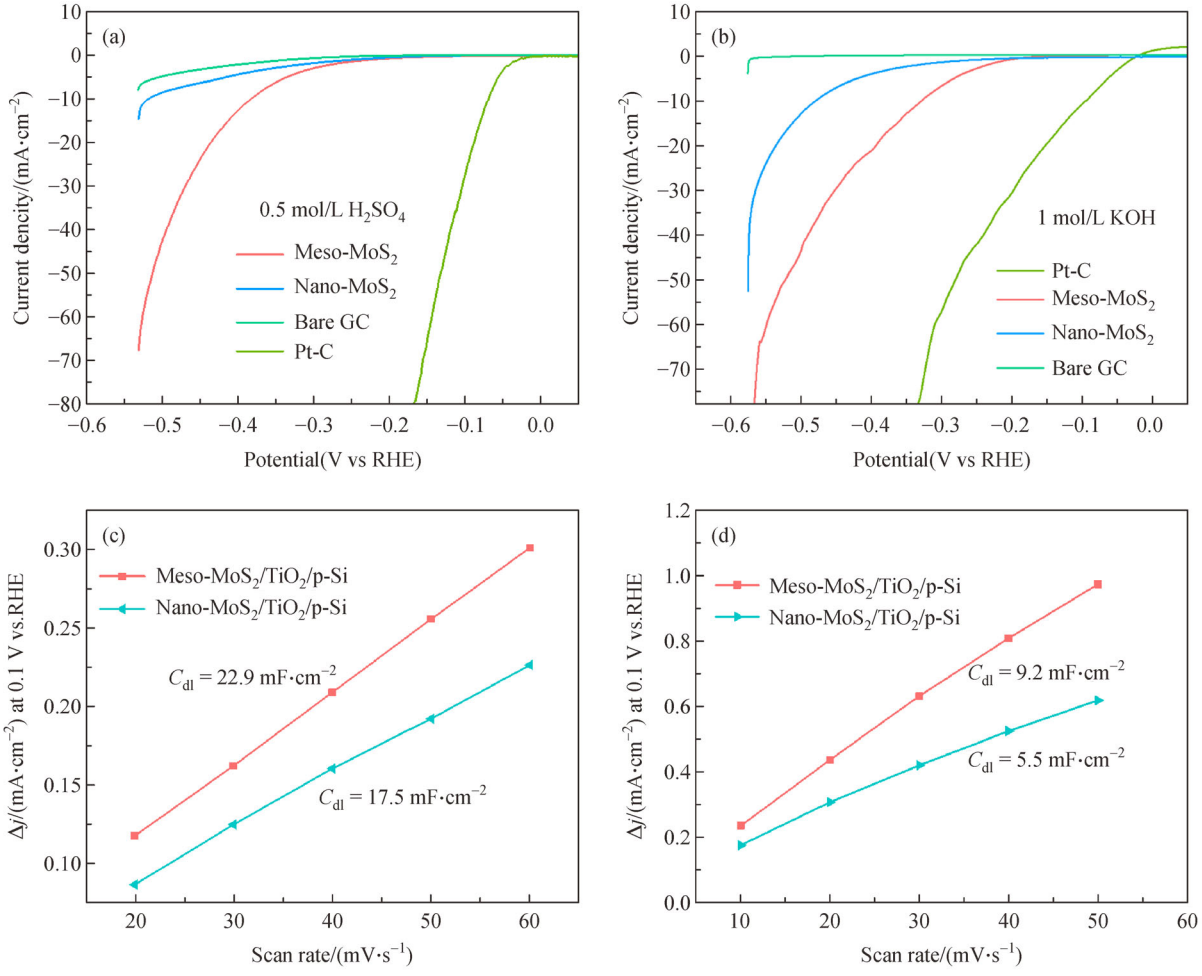

Fig. 5 HER electrocatalytic performance of the cocatalysts.
(a) Polarization curves of various catalysts in 0.5 mol/L H_2SO_4; (b) polarization curves of various catalysts in 1.0 mol/L KOH; (c) current densities as a function of the scan rate for meso-MoS_2 and nano-MoS_2 in 0.5 mol/L H_2SO_4 at 0.1 V versus RHE; (d) current densities as a function of the scan rate for meso-MoS_2 and nano-MoS_2 in 1.0 mol/L KOH at 0.1 V versus RHE.

Acknowledgements This work was supported by the National Natural Science Foundation of China (Grant Nos. 51672174, 51779139, 51772190, and 51972210) and the Advanced Energy Material and Technology Center of Shanghai Jiao Tong University, China.

Electronic Supplementary Material Supplementary material is available in the online version of this article at https://doi.org/10.1007/s11708-021-0783-7 and is accessible for authorized users.

References

1. Strandwitz N C, Turner-Evans D B, Tamboli A C, et al. Photoelectrochemical behavior of planar and microwire-array Si|GaP electrodes. Advanced Energy Materials, 2012, 2(9): 1109–1116
2. Yue P, She H, Zhang L, et al. Super-hydrophilic CoAl-LDH on $BiVO_4$ for enhanced photoelectrochemical water oxidation activity. Applied Catalysis B: Environmental, 2021, 286: 119875
3. Li Y, Yang Y, Huang J, et al. Preparation of CuS/$BiVO_4$ thin film and its efficacious photoelectrochemical performance in hydrogen generation. Rare Metals, 2019, 38(5): 428–436
4. Sun K, Shen S, Liang Y, et al. Enabling silicon for solar-fuel production. Chemical Reviews, 2014, 114(17): 8662–8719
5. Liu D, Ma J, Long R, et al. Silicon nanostructures for solar-driven catalytic applications. Nano Today, 2017, 17: 96–116
6. Fan R, Zhou J, Xun W, et al. Highly efficient and stable Si photocathode with hierarchical MoS_2/Ni_3S_2 catalyst for solar hydrogen production in alkaline media. Nano Energy, 2020, 71: 104631
7. Li H, Wang T, Liu S, et al. Controllable distribution of oxygen vacancies in grain boundaries of p-Si/TiO_2 heterojunction photocathodes for solar water splitting. Angewandte Chemie, 2021, 133 (8): 4080–4083
8. Zheng J, Lyu Y, Wang R, et al. Crystalline TiO_2 protective layer with graded oxygen defects for efficient and stable silicon-based photocathode. Nature Communications, 2018, 9(1): 3572
9. Zhou X, Liu R, Sun K, et al. Interface engineering of the photoelectrochemical performance of Ni-oxide-coated n-Si photo-

anodes by atomic-layer deposition of ultrathin films of cobalt oxide. Energy & Environmental Science, 2015, 8(9): 2644–2649
10. Fu Q, Wang W, Yang L, et al. Controllable synthesis of high quality monolayer WS_2 on a SiO_2/Si substrate by chemical vapor deposition. RSC Advances, 2015, 5(21): 15795–15799
11. Xun W, Wang Y, Fan R, et al. Activating the MoS_2 basal plane toward enhanced solar hydrogen generation via *in situ* photoelectrochemical control. ACS Energy Letters, 2021, 6(1): 267–276
12. Fan R, Dong W, Fang L, et al. More than 10% efficiency and one-week stability of Si photocathodes for water splitting by manipulating the loading of the Pt catalyst and TiO_2 protective layer. Journal of Materials Chemistry A, Materials for Energy and Sustainability, 2017, 5(35): 18744–18751
13. Li F, Yuan Y, Feng X, et al. Coating of phosphide catalysts on p-silicon by a necking strategy for improved photoelectrochemical characteristics in alkaline media. ACS Applied Materials & Interfaces, 2021, 13(17): 20185–20193
14. Lin H, Li S, Yang G, et al. *In situ* assembly of MoS_x thin-film through self-reduction on p-Si for drastic enhancement of photoelectrochemical hydrogen evolution. Advanced Functional Materials, 2021, 31(3): 2007071
15. Seger B, Pedersen T, Laursen A B, et al. Using TiO_2 as a conductive protective layer for photocathodic H_2 evolution. Journal of the American Chemical Society, 2013, 135(3): 1057–1064
16. Chen C J, Veeramani V, Wu Y H, et al. Phosphorous-doped molybdenum disulfide anchored on silicon as an efficient catalyst for photoelectrochemical hydrogen generation. Applied Catalysis B: Environmental, 2020, 263: 118259
17. Wang H, Zhang L, Chen Z, et al. Semiconductor heterojunction photocatalysts: design, construction, and photocatalytic performances. Chemical Society Reviews, 2014, 43(15): 5234
18. Li S, Zhang P, Song X, et al. Photoelectrochemical hydrogen production of TiO_2 passivated Pt/Si-nanowire composite photocathode. ACS Applied Materials & Interfaces, 2015, 7(33): 18560–18565
19. Fu H, Varadhan P, Tsai M L, et al. Improved performance and stability of photoelectrochemical water-splitting Si system using a bifacial design to decouple light harvesting and electrocatalysis. Nano Energy, 2020, 70: 104478
20. Zhu L, Lin H, Li Y, et al. A rhodium/silicon co-electrocatalyst design concept to surpass platinum hydrogen evolution activity at high overpotentials. Nature Communications, 2016, 7(1): 12272
21. Liu J, Wu H, Li F, et al. Recent progress in non-precious metal single atomic catalysts for solar and non-solar driven hydrogen evolution reaction. Advanced Sustainable Systems, 2020, 4(11): 2000151
22. Hu C, Zhang L, Gong J. Recent progress made in the mechanism comprehension and design of electrocatalysts for alkaline water splitting. Energy & Environmental Science, 2019, 12(9): 2620–2645
23. Ding Q, Meng F, English C R, et al. Efficient photoelectrochemical hydrogen generation using heterostructures of Si and chemically exfoliated metallic MoS_2. Journal of the American Chemical Society, 2014, 136(24): 8504–8507
24. Kwon K C, Choi S, Lee J, et al. Drastically enhanced hydrogen evolution activity by 2D to 3D structural transition in anion-engineered molybdenum disulfide thin films for efficient Si-based water splitting photocathodes. Journal of Materials Chemistry A, Materials for Energy and Sustainability, 2017, 5(30): 15534–15542
25. Wang H, Xiao X, Liu S, et al. Structural and electronic optimization of MoS_2 edges for hydrogen evolution. Journal of the American Chemical Society, 2019, 141(46): 18578–18584
26. Kiriya D, Lobaccaro P, Nyein H Y Y, et al. General thermal texturization process of MoS_2 for efficient electrocatalytic hydrogen evolution reaction. Nano Letters, 2016, 16(7): 4047–4053
27. Karunadasa H I, Montalvo E, Sun Y, et al. A molecular MoS_2 edge site mimic for catalytic hydrogen generation. Science, 2012, 335 (6069): 698–702
28. Wang W, Zhu S, Cao Y, et al. Edge-enriched ultrathin MoS_2 embedded yolk-shell TiO_2 with boosted charge transfer for superior photocatalytic H_2 evolution. Advanced Functional Materials, 2019, 29(36): 1901958
29. Kibsgaard J, Chen Z, Reinecke B N, et al. Engineering the surface structure of MoS_2 to preferentially expose active edge sites for electrocatalysis. Nature Materials, 2012, 11(11): 963–969
30. Li X, Li Y, Wang H, et al. Fabrication of a three-dimensional bionic Si/TiO_2/MoS_2 photoelectrode for efficient solar water splitting. ACS Applied Energy Materials, 2021, 4(1): 730–736
31. Li F, Wang C, Han X, et al. Confinement effect of mesopores: *in situ* synthesis of cationic tungsten-vacancies for a highly ordered mesoporous tungsten phosphide electrocatalyst. ACS Applied Materials & Interfaces, 2020, 12(20): 22741–22750
32. Rasamani K D, Alimohammadi F, Sun Y. Interlayer-expanded MoS_2. Materials Today, 2017, 20(2): 83–91
33. Tsai C, Abild-Pedersen F, Nørskov J K. Tuning the MoS_2 edge-site activity for hydrogen evolution via support interactions. Nano Letters, 2014, 14(3): 1381–1387
34. Fan R, Mao J, Yin Z, et al. Efficient and stable silicon photocathodes coated with vertically standing nano-MoS_2 films for solar hydrogen production. ACS Applied Materials & Interfaces, 2017, 9(7): 6123–6129